Experimental and Numerical Investigations of Noise from Micro Turbojet Engine

Tamer M. Raef[a], Aly Elzahaby[b], S. Abdallah[c], Mohamed K. Khalil[d] and S.Wagdy[e]

Abstract— Jet noise remains a significant noise component in modern aero-engines. A high-speed flow mixing with the surrounding air constitutes noise sources behind the nozzle. Since experimental activities on real aeronautical engines can be very complex and expensive, the use of parts of real engines or small-size turbojets can be very useful for research activities. The present paper describes a test rig constructed for the study of jet noise from Jet Cat micro turbojet engine used for unmanned aerial vehicles (UAV) with a nominal thrust of 230 N at 112000 rpm. The aim is to investigate the near field noise generated by turbulent high subsonic single stream jet at different exit Mach numbers (0.4, 0.7, and 0.8). The overall sound pressure levels and pressure spectra are measured using 6 B&K ½ inch condenser microphones. The microphones are mounted on a linear rake that is setup outside the flow field to account for the growth of the shear layer. The measurements of noise source distribution along the length of the high-speed jet are taken at a grid of six axial and five radial positions. All the test instrumentation, data acquisition system and detailed measurements are presented. The data show that the peak overall sound pressure levels are observed at axial position X= 2.5-7.5 jet diameters with different radial positions. In addition, numerical solutions are obtained using three-dimensional unsteady- Reynolds-averaged Navier–Stokes equations based on the RSM turbulence model. The commercial CFD code FLUENT 15.0 is used for both flow field and noise predictions. The computational grid consists of hexahedral numerical mesh containing more than four million nodes. Grid resolution sensitivity is verified using a two-dimensional, axisymmetric slice of coarse and fine meshes. The numerical results show good agreement with the experimental measurements. The results of this study will be utilized for finding methods of noise reduction in high subsonic single-stream jet engines.

Index Terms—: Aeroacoustics, jet noise, CFD simulation, turbojet engine

1 Introduction

The number of commercial aircraft in service is continuously growing, and airports around the world are growing in size, which increases exposure to air traffic noise in populated areas[1]. Military aircraft have engines with noise characteristics much louder than civilian aircraft due to their very low bypass ratios and high exit temperatures and velocities of the jets. They are designed with variable-geometry nozzles to provide optimal thrust in different operating conditions. The resulted increased noise poses a health threat to ground crews as well as causing an annoyance to communities in the vicinity of military airbases [2]. Threshold values for noise certification of new aircraft are based on global restrictions on noise generated by air traffic. Moreover, local restrictions for airports with heavy traffic limit operating hours or even impose direct noise penalty costs. Engine noise refers to noise generated by the turbo-machinery and jet exhaust. A strong component of engine noise is the jet noise that is generated from the turbulent mixing within the shear flow between the jet exhaust and ambient medium [3].

Many experimental investigations have been carried out to study the various characteristics of near field noise from Simple round nozzles [4], [5], [6]. A new methodology for using data obtained on nozzles from testing small scale at Pennsylvania State University (PSU) and moderate scale at NASA Glenn Research Center, supported by computations, to reliably predict the full-scale engine noises. The experimental results presented show reasonable agreement between small-scale and medium-scale jets, as well as between heated jets and heat simulated one [2]. A 1/150th scale model, based on the exit geometry typically found on commercial jet engines, was designed and manufactured at Warwick. The laboratory jet flow conditions operated at 0.7 Mach. The work presented in this study looks at the noise generated in a subsonic, co-flowing jet, with particular focus given to the distribution of sound sources from 5 kHz to 80 kHz [7]. Jet noise was studied from the development and acoustic validation of the Small Hot Jet Aeroacoustic Rig (SHJAR). The rig has been designed and developed using the best practices of the industry. The measured 'baseline' jet noise spectra agree to within the repeatability of similar nozzles tested in historic rigs [8].

In recent years there has been much interest in the development of Reynolds-averaged, Navier-Stokes (RANS) based jet noise prediction schemes. While the details of individual approaches vary, such schemes always seek to use the output of a RANS calculation (typically based on a k-ϵ turbulence model) as input to a noise calculation. RANS-based noise prediction scheme was developed by introducing a new scale based on the turbulence energy transfer rate. The results showed that the new frequency dependant time scale proposed significantly improved the noise predictions for isothermal jets [9]. Another study modified a physics-based jet noise prediction methodology based on RANS input to improve the noise prediction for heated subsonic jets [10]. A clear attraction of these approaches is the relative speed of the calculation

[a] *Corresponding author is currently pursuing PhD degree program in Military Technical College (MTC), Egypt, tamerraef1@gmail.com, tamer.shahen@uc.edu.*
[b] *Professor, Depart of Mechanical Power Engineering, Tanta University, Tanta, Egypt, elzahaby47@gmail.com.*
[c] *Professor, Department of Aerospace Engineering and Engineering Mechanics, University of Cincinnati, Cincinnati, Ohio 45221-0070, USA, shaaban.abdallah@uc.edu.*
[d] *Doctor, Military Technical College (MTC), Cairo, Egypt, khilo99@yahoo.com*
[e] *Doctor, Military Technical College (MTC), Cairo, Egypt, samer_guirguis_2000@yahoo.com*

compared to using large eddy simulation (LES). On the other hand, the failure of RANS models to yield accurate off-design aerodynamic, mixing predictions, and noise source information, has resulted in the increasing use of LES as the basis for noise predictions. Added impetus for the use of LES has also resulted from the recent increase in affordable computing power. LES resolves only the dynamically important flow scales and models the effects of smaller scales. However, it is also possible to use unsteady RANS methods to compute the noise of the largest flow features. The simulation domain must be sufficiently large to include all the sound sources of interest and at least part of the acoustic near field [11].

Unfortunately, analysis and measurements on real aeronautical turbines are complex and expensive, and for this reason the use of parts of real engines or small size turbojets can be very interesting for research activities. Several examples exist of small-size turbojet-engines that have been developed and produced in particular for unmanned aerial vehicles (UAV). Some for research purposes by Universities and Research Institutions [12], and some for education and scientific activities by specialized industries, such as the SR30 turbojet produced by Turbine Technologies. For military applications, the use of UAV's has seen a significant increase over the last two decades. One of the many classes of propulsion devices used in UAV's is that of micro gas turbine engines [13].

This paper consists of two parts: The first part describes the experimental data conducted on a designed test rig for predicting the near-field noise of the high speed exhausts from micro turbojet engine. This is examined in terms of overall sound pressure levels and pressure spectra at various test conditions. The second part describes the numerical modeling using the commercial CFD code FLUENT 15.0 for both flow field and noise predictions, and then uses both experiments and simulations to understand sources of jet noise.

2 Experimental Work

The Jet Cat P200-SX Gas Turbine Engine as shown in Fig.1 was the primary focus of this study [14]. The engine in the test cell performs all the basic functions of full-scale turbine engines. These engines have been selected mainly because of their simple setup, low maintenance, and a wide variety of application for gas turbine engine [15]. The maximum thrust of the engine used is 230 N at 112,000 RPM of rotor rotational speed.

2.1 Engine description

The Jet Cat is a single spool turbojet. It is comprised of a standard inlet, a single stage centrifugal compressor with vane diffusers, an annular combustor, a single stage axial turbine and convergent nozzle. Two types of fuel are used, propane during the startup and Jet-A1 fuel for normal runs which are normally automated via an Engine Control Unit (ECU). The engine, when supplied with propane gas start, is equipped with a check valve at the engine itself. This will ensure that no pressure can escape through the gas run, engine operation parameters and gas properties at the different stages along the air path can be determined by using the various instruments and data acquisition systems.

After the turbine has ignited on propane, the starter motor further accelerates the turbine. At approx. 5000 RPM, the fuel pump is automatically started at minimum power by the ECU. Beginning from this first pump start voltage, the fuel flow is then slowly increased by increasing the pump voltage. The engine begins to accelerate as soon as fuel begins to burn, and the power of the pump increases through the time at the "fuel ramp" slope. The engine continues accelerating alone until the idle rpm is reached. Fuel must be mixed with 5% synthetic turbine oil. The Power Supply for all electrical components of the turbine (starter / glow plug / ECU / fuel pump / fuel and gas valves) are supplied by the six-cell, 2400 mAh ECU battery. ECU monitors all of the controls necessary to guarantee that the engine stays at the user defined parameters of operation. It is also providing failsafe shutdown of the engine when it detects any important abnormality. The Ground Support Unit (GSU) serves as a terminal for displaying and programming turbine parameters. The LED I/O (Input/output) board is a connection point for the data bus and a display for the current status of the ECU. The board should be mounted with the LED's visible and the data bus connector accessible for plugging in the GSU [14]. The electrical connection diagram was shown in Fig.2.

Fig. 1. Jet Cat P200-SX Gas Turbine Engine

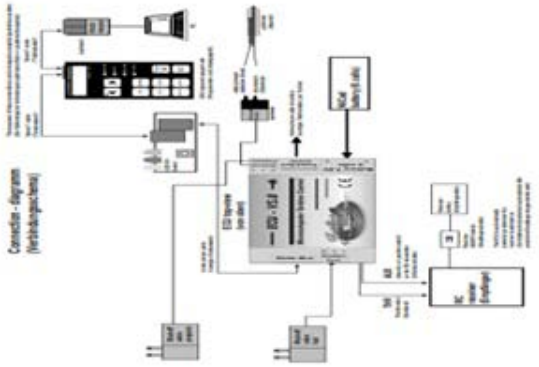

Fig. 2. Electrical connection diagram of Jet Cat, [14].

2.2 Test Stand and Instrumentation

A purpose built, mobile test stand was constructed for the Jet Cat engine. The stand has a facility that when thrust generates, engine stand moves so that it forces compression to load cell. The stand was mounted on a plate. It consisted of an ECU, power supplies, instrumentation and associated hardware. The main pump supplies fuel from the main tank to a buffer tank beneath the test stand [16].

The engine was instrumented with a K-type thermocouple mounted in the exhaust nozzle. Fuel flow is measured by a flow meter (Omega FLR-1010-ST-D) set in line with the engine fuel pump. Engine speed is measured using a Hall Effect sensor. As the shaft rotates, the Hall Effect sensor picks up the magnetic flux created by the magnet. A pulse signal is then sent to the ECU for rpm readout. The engine thrust is measured by using a compression load cell (Omega LC304-100). The data acquisition device used is OMB-DAQ-56 hardware which has high performance and flexibility as modular type instrument with that for convenience of data logger and low cost advantage. The experimental analysis permitted the thrust and fuel flow rates to be obtained at the most important stations of the cycle at different exit Mach number ranging from 0.4 to 0.8.

2.3 Noise Measurements

A test stand is designed and constructed for acoustic measurements and connected with the engine as shown in Fig.3. In order to map the near-field acoustic measurements, 6 B&K ½ inch condenser microphone (Type- 4190) are mounted on a linear rake which is in turn mounted on a large three-axis traverse. The rake relative to the core nozzle is setup to be outside the flow field to account for the growth of the shear layer. The microphones are connected with B&K preamplifiers (Type - 2669). They are first calibrated using a B&K calibration instrument (Type-4230) such that it records a 94 dB at a frequency of 1 kHz when the instrument operated [17]. The pressure and acoustic signals were acquired using a National Instruments digital data acquisition cards NI-9234 (8- channel, 5V, 24- Bit software - selectable IEPE). All measuring sensors are connected to the DAQ (Data Acquisition) and the logging data are used as function parameters of the program, Lab VIEW [18].

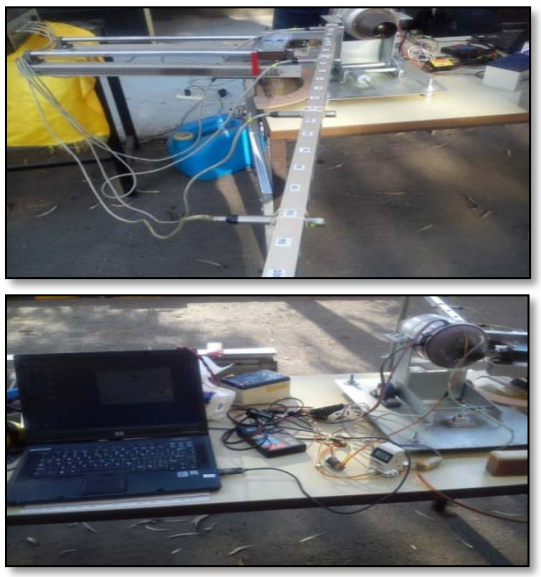

Fig. 3. Test stand for acoustic measurements

3. Results and Discussion

The microphones are placed at various axial positions from X/ Dj = 0.5-12.5 (where X is the axial distance from the jet exit, Dj is the exit diameter of circular convergent nozzle).The microphones rake is stepped through a rectangular region just outside the main flow region at five radial positions(R): 2Dj, 4Dj, 6Dj, 8Dj and 11Dj. All noise measurements are made at different axial, radial positions and at different exit Mach numbers 0.4, 0.7 and 0.8.

Fig.4, Fig.5, Fig.6, Fig.7, Fig.8 and Fig.9. Compare the near-field sound pressure level (SPL) spectra at different axial positions from X/Dj = 0.5-12.5. The results are obtained at three different exit Mach numbers and at R=2 Dj. The spectra cover a frequency range from 100 Hz to 20 kHz. For all axial positions, the near-field sound pressure level amplitude increases as exit Mach number increases with the spectra displaying its broadband nature without any dominant peaks. However, the increase is larger in the acoustic region of the spectrum while there is not much change for the hydrodynamic region. This implies that the large-scale structures for the different Mach number jets are fairly similar in frequency and only slightly different in amplitude.

Fig.10, Fig.11, Fig.12, Fig.13, Fig.14 and Fig.15 compare the near-field sound pressure level (SPL) spectra for the exit Mach 0.8 case at different radial positions (R=2-11Dj) and different axial positions. At each microphone position, the spectrum has a single peak whose magnitude decreases with increasing distance from the shear-layer. For the near-field array (R = 2Dj, 4Dj, 6Dj, 8Dj and 11Dj), it is noticed the decay of the hydrodynamic pressure for increasing R. For all radial positions, a clear transition is seen from a region of large hydrodynamic pressure (R=2Dj) to a region where the hydrodynamic pressure has much lower amplitude (R=11Dj). As the distance of the near field microphone from the jet shear-layer is increased, the magnitude of the cross-spectra for a given microphone decreases and becomes slightly broader, whereas the phase of a given microphone becomes more linear. The reduction in cross-spectral magnitude as the near field microphone is moved away from the shear-layer is likely due to the loosely spherical acoustic wave decay.

The resulting grid of pressure fluctuations data can then be analyzed on an overall sound pressure level (OASPL) basis and can be mapped to look at source location and direction of propagation. Fig.16 compares the contours of the near field OASPL at different exit Mach number with respect to different axial and radial microphones positions. It is noticed here that OASPL increases as Mach number increases at the same axial and radial positions. Peak OASPL is observed at X= 2.5-7.5 Dj, for different radial positions. The key emphasis here is the presence of large-scale features

which is strongly related to the correlation between the velocity and pressure field. The correlation is significant for both velocity components, and the amplitude distribution of the correlation is highly dependent on the radial position of the microphone array. Near the jet (R=2Dj), the highest amplitudes are localized around the microphone that is most influential for the estimate being presented. The biggest difference between the radial positions is that for R=2Dj, there is higher amplitudes near the nozzle exit compared to the near nozzle region for the other radial positions.

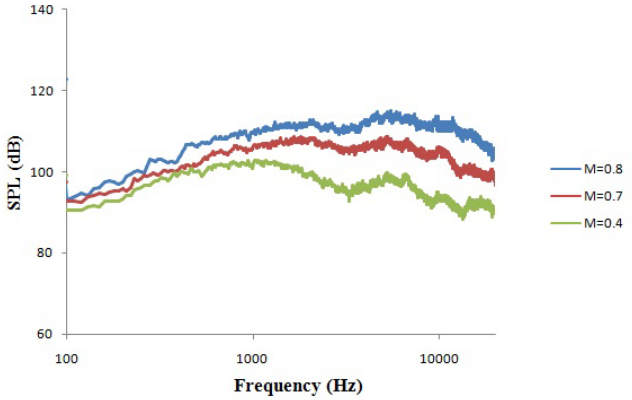

Fig. 4. SPL at different Mach number and (X/Dj=0.5)

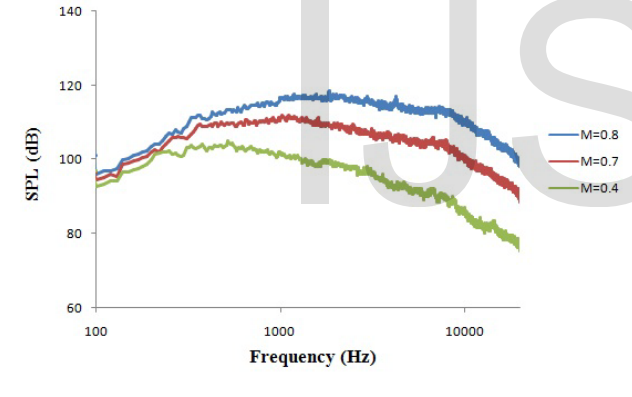

Fig. 5. SPL at different Mach number and (X/Dj=2.5)

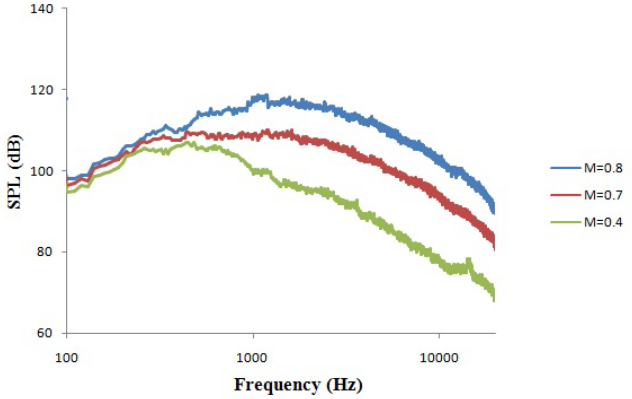

Fig. 6. SPL at different Mach number and (X/Dj=5)

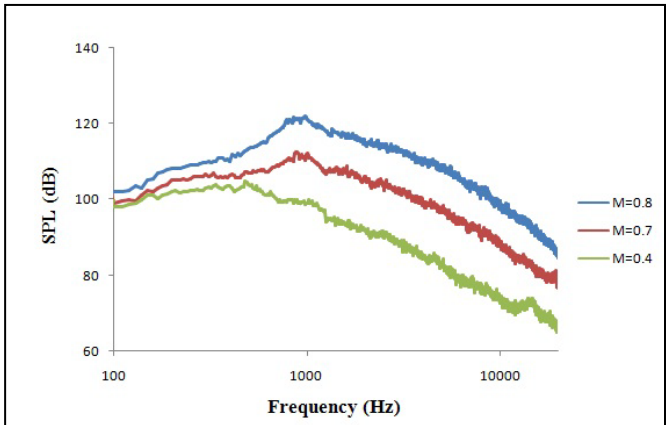

Fig. 7. SPL at different Mach number and (X/Dj=7.5)

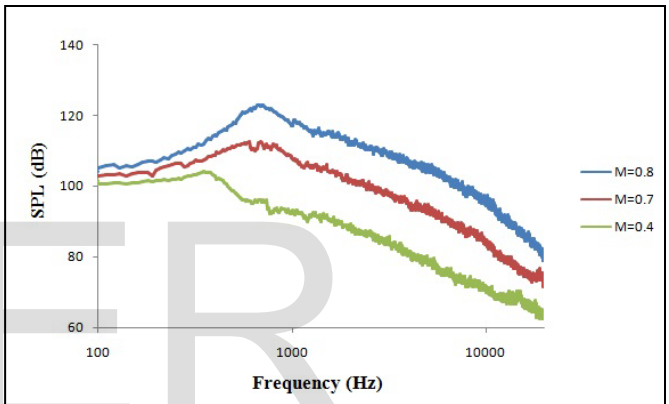

Fig. 8. SPL at different Mach number and (X/Dj=10)

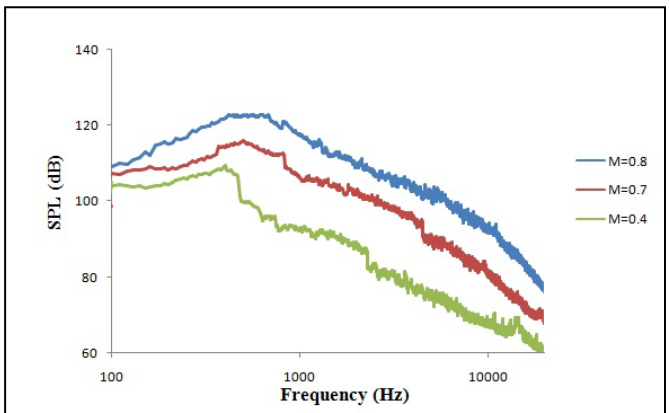

Fig. 9. SPL at different Mach number and (X/Dj=12.5)

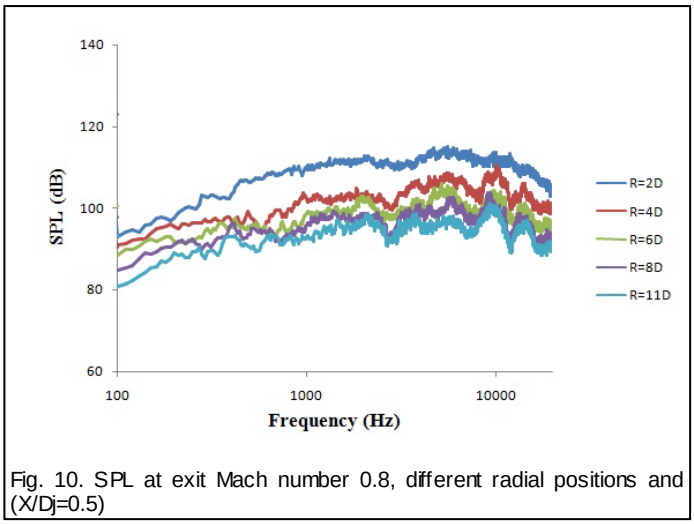

Fig. 10. SPL at exit Mach number 0.8, different radial positions and (X/Dj=0.5)

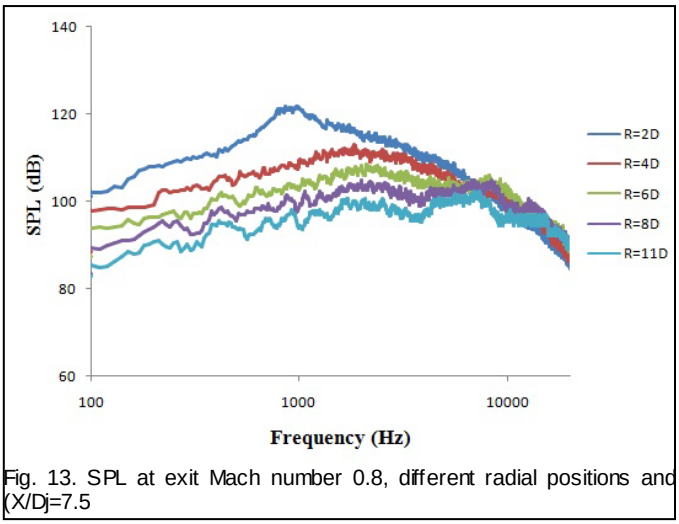

Fig. 13. SPL at exit Mach number 0.8, different radial positions and (X/Dj=7.5

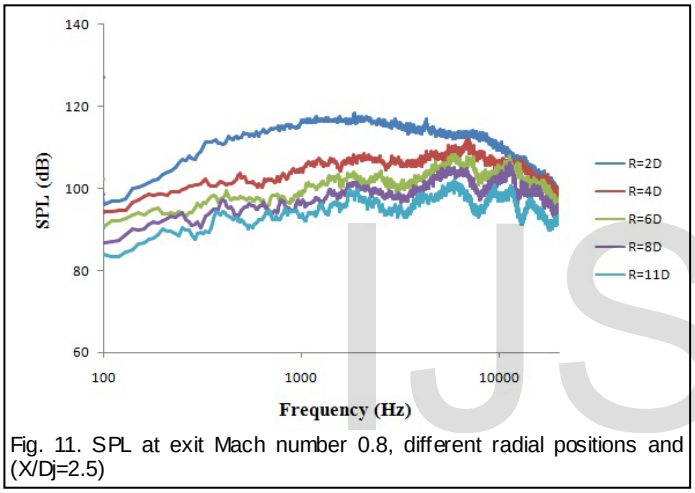

Fig. 11. SPL at exit Mach number 0.8, different radial positions and (X/Dj=2.5)

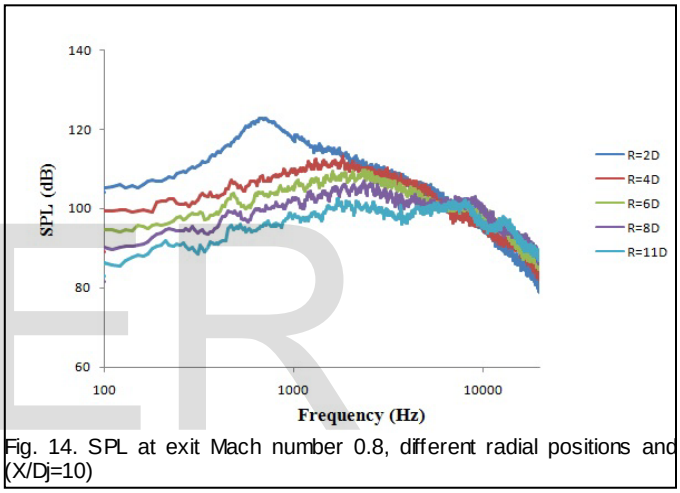

Fig. 14. SPL at exit Mach number 0.8, different radial positions and (X/Dj=10)

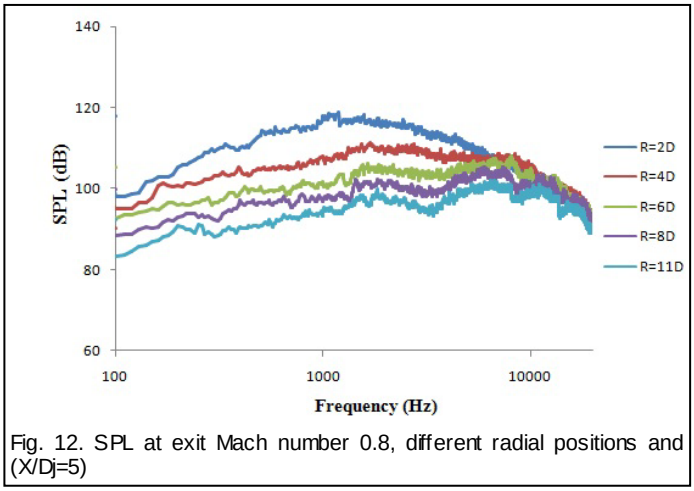

Fig. 12. SPL at exit Mach number 0.8, different radial positions and (X/Dj=5)

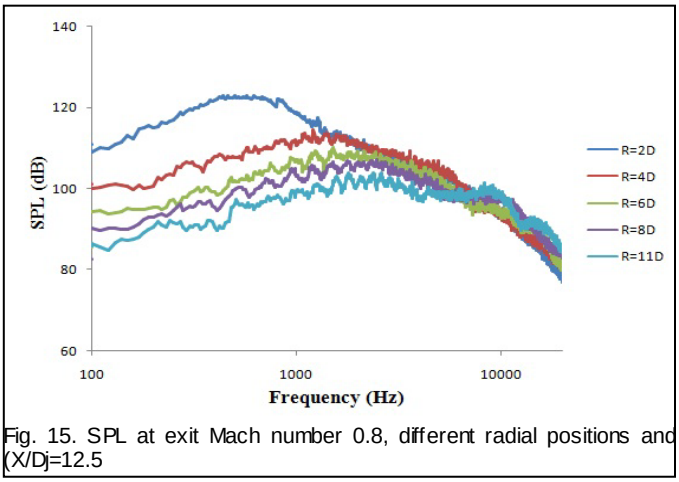

Fig. 15. SPL at exit Mach number 0.8, different radial positions and (X/Dj=12.5

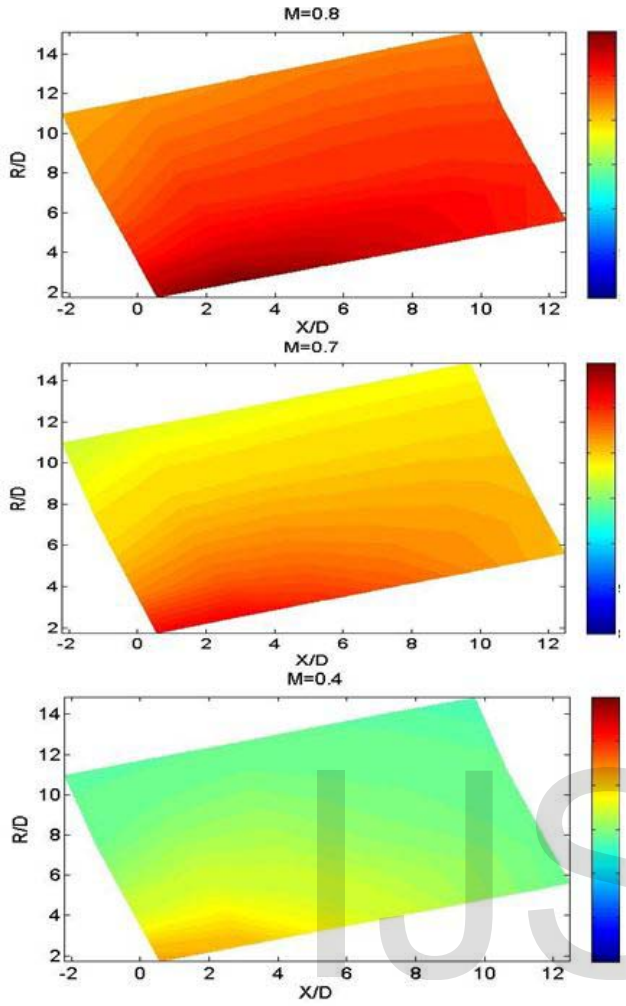

Fig. 16. Contours of near-field OASPL in dB at different exit Mach numbers

4 Aeroacoustic Modeling

The aeroacoustic behavior can be completely characterized by solving the compressible Navier-Stokes equations. In other words, aeroacoustic phenomena can be explained through the use of the principles of mass, momentum and energy conservation. For simple problems, direct numerical simulations that solve the compressible Navier-Stokes equations are able to solve for both the aerodynamic flow field and the acoustic field. However, for problems in industrial applications, this approach becomes extremely difficult due to the fact that the acoustic energy is usually several orders of magnitude smaller than the hydrodynamic energy. The length and time scales of the two fields are therefore not compatible, and the need to separate the two fields becomes apparent [11].

4.1 Computational Domain and Grid Generation

Three dimensional Unsteady- Reynolds-averaged Navier–Stokes based methods (URANS) calculations using the commercial CFD code FLUENT 15.0 is used for both flow field and noise predictions. The commercial code is used to model the aerodynamic flow as well as the jet noise emissions, with the accuracy of the various predictive approaches assessed by comparison with available experimental data. The natural symmetry of the nozzle allows consideration of a cylindrical computational domain. The computational domain starts from the nozzle outlet and does not include the nozzle shape. A three dimensional hexahedral numerical mesh containing more than four million nodes is used for the numerical simulation. The mesh is refined near the nozzle lip region and expanded in the downstream and radial directions. After a set of sample two-dimensional runs are performed, where the mesh resolution is varied, the operational grid consisted of 45k nodes (50 nodes stretched along the inner radius of the nozzle with an expansion ratio 0.99, 152 nodes used along the edge of the domain starting from the nozzle up to the end of the domain and 190 nodes were used along the axis of the jet for a distance 900mm, with an expansion ratio of 0.99 and 0.98 up to 1500mm). The three dimensional grid was built by rotating a 2D slice about the jet axis. Hence, the final three-dimensional grid contains approximately 4.3 million nodes and was performed using a parallelizing technique on a twelve-processor computer in order to obtain a converged solution.

4.2 Acoustic Results and Discussion

The simulation results for the velocity field components are presented in Fig.17 and Fig.18. The three-dimensional results predict well the mean velocity component. However the R.M.S. velocity component is modeled better in the three dimensional case, in particular in the region close to the jet axis where no assumptions about the symmetry of the problem are made. Fig. 19 shows the contours of the near field OASPL at exit Mach number 0.8 with respect to different axial and radial microphones positions. Peak OASPL is observed at X= 2-7 Dj. The results are compared with the experimental data in Fig. 16. The details are presented at the different radial positions as shown in Fig.20, Fig.21, Fig.22, Fig.23 and Fig.24. Pressure distributions and near-field noise intensities obtained from the simulations show good agreement with those obtained from the experimental measurements.

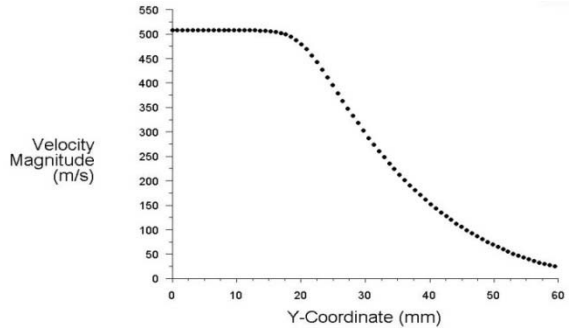

Fig. 17. Predictions of the radial profile of the velocity magnitude at a downstream distance of 3Dj obtained with URANS in 3D.

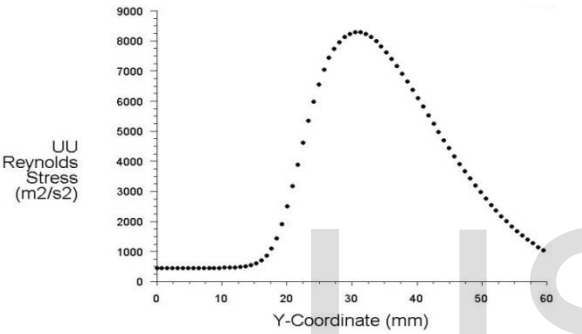

Fig. 18. Predictions of the axial normal stress at a downstream distance of 3Dj obtained with URANS in 3D.

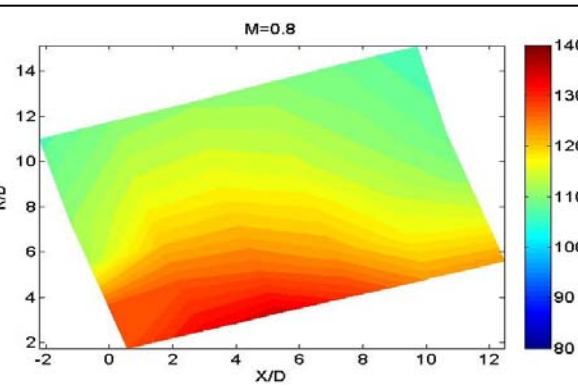

Fig. 19. Contours of near-field OASPL in dB at M=0.8(numerical)

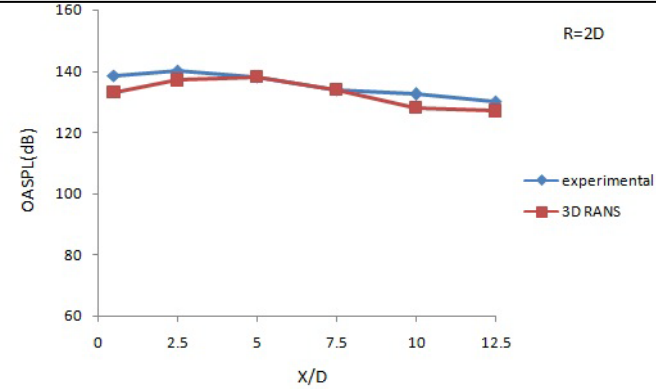

Fig. 20. Comparison between measurements and numerical results at R=2Dj

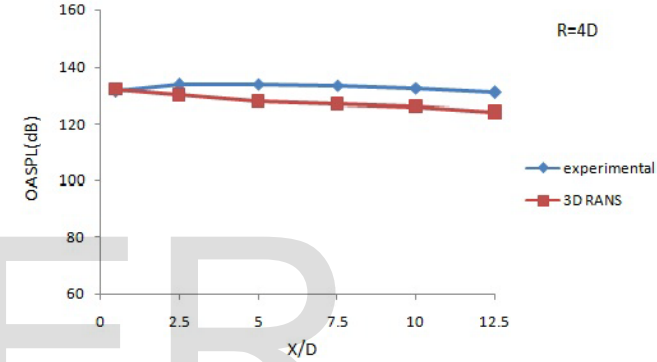

Fig. 21. Comparison between measurements and numerical results at R=4 Dj.

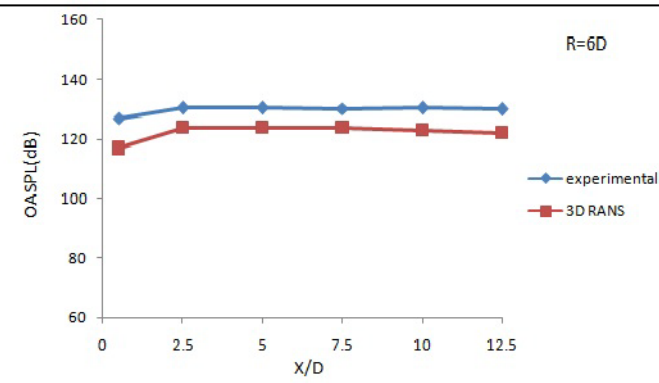

Fig. 22. Comparison between measurements and numerical results at R=6 Dj

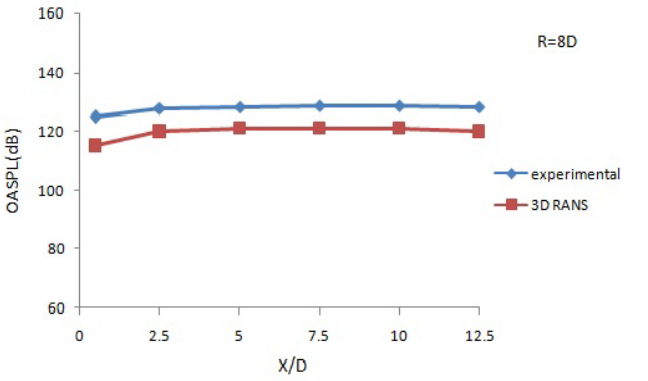

Fig. 23. Comparison between measurements and numerical results at R=8 Dj

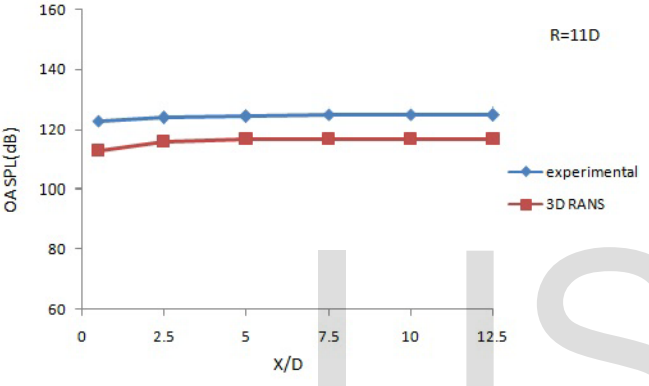

Fig. 24. Comparison between measurements and numerical results at R=11 Dj

5. Conclusions

A test rig is designed and constructed for the near field acoustic measurements. Experimental data exploring the noise generated by turbulent, high subsonic, single-stream jet from Jet Cat micro turbojet engine are presented. Noise source distributions are investigated for a wide range of exit jet Mach number ($0.4 \leq M_j \leq 0.8$). 6 B&K ½ inch condenser microphone mounted on a linear rake are used for noise measurements at different axial and radial positions. The overall sound pressure level increases as Mach number increases at the same axial and radial positions. However, the increase is larger in the acoustic region of the spectrum which implies that the large-scale structures for the different exit Mach number are fairly similar in frequency and only slightly different in amplitude. It is also noticed the decay of the hydrodynamic pressure for increasing R. For all radial positions, a clear transition is seen from a region of large hydrodynamic pressure (R=2 Dj) to a region of lower hydrodynamic pressure (R=11 Dj). Peak OASPL is observed at X= 2.5-7.5 Dj, for different radial positions. The key emphasis here is the presence of large-scale features which are strongly related to the correlation between the velocity and pressure field and related to the wavelength of the large-scale structures which increased downstream. The numerical results are predicted by solving the URANS equations for compressible flow using ANSYS FLUENT 15.0. Pressure distributions and near-field noise obtained from the simulations show good agreement with those obtained from the experimental measurements. This good agreement shows that numerical simulations and measurements can play complementary roles in the investigation of methods of noise reduction.

References

[1] N. Andersson, "A Study of Subsonic Turbulent Jets and Their Radiated Sound Using Large-Eddy Simulation," PhD thesis, Chalmers University of Technology, Sweden, 2005.
[2] J. V. a. D. K. M. Ching-Wen Kuo, "Acoustic measurements of models of military style supersonic nozzle jets," Chinese Journal of Aeronautics, 2014.
[3] S. Mayoral, "Prediction of jet noise shielding with forward flight effects," PhD thesis, Mechanical and Aerospace Engineering, University of California, Irvine, 2013.
[4] A. K. a. I. C. Rajan Kumar, "Near-Field Acoustic Characteristics of a Turbulent Axisymmetric Pulsed Jet," AIAA, vol. 48, 2012.
[5] K. V. Tam Christopher, K. K. Ahuja and J. Panda, "The sources of jet noise: experimental evidence," Journal of Fluid Mechanics, vol. 615, pp. 253-292, 2008.
[6] B. Callender, E. Gutmark and S. Martens, "Near-Field Investigation of Chevron Nozzle Mechanisms," AIAA, vol. 46, pp. 36-45, 2008.
[7] A. Kiran, "Jet Noise: Aeroacoustic Distribution Of A Subsonic Co-Axial Jet," PhD thesis, University of Warwick, UK, 2008.
[8] J. B. a. C. A. Brown, "Validation of the Small Hot Jet Acoustic Rig for Jet Noise Research,", NASA, 2006.
[9] M. a. S. Azarpyvand, R., "Noise prediction of a short-cowl jet using energy transfer rate time-scale,", 14th AIAA/CEAS Aeroacoustics Conference, 2008.
[10] A. Khavaran, and Kenzakowski, D.C., "Progress towards improving jet noise predictions in hot jets,", 13th AIAA/CEAS Aeroacoustics Conference, 2007.
[11] M. F. a. M. P. T. Stanko. D. B. Ingham, "Application of rans and fwh modelling to the prediction of noise from round jets," ASME, 2009.
[12] P. N. a. A. S. M. Badami, "Experimental and numerical analysis of a small-scale turbojet engine," Energy Conversion and Management, vol. 76, 2013.
[13] W. S. A. Zafer Leylek, Glen Rowlinson and Nigel Smith, "An investigation into performance modeling of a small gas turbine engine ", ASME, 2013.
[14] US. Patent, "Jet Cat instruction manual," 2008.
[15] J. K. Seonghee Kho, Miyoung Park, Changduk Kong and Kyungjae Lee, "Development of condition monitoring test cell using micro gas turbine engine " , ASME, 2009.
[16] N. T. Tatsuya Ishii, Hideshi Oinuma and Tsutomu Oishi, "Hot-jet noise test of a revised notched nozzle," ASME, 2012.
[17] S. S. AlGattus, "Experimental Investigation of Noise Reduction in Supersonic Jets due to Jet Rotation and to Nozzle Geometry Changes", Mechanical engineering, Concordia University, Montreal, 1999.
[18] H. B. Park, "Lab VIEW 8 Graphical Programming" Jungik Publishing Co., 2008.